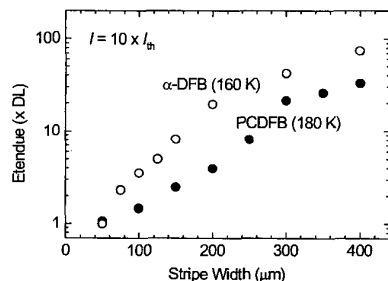


**CTuE3 Fig. 2.** PCDFB laser emission spectra at several operating temperatures, for pulsed optical pumping with a 200-μm-wide Gaussian stripe pumped at five times the lasing threshold. The spectra for Fabry-Perot lasers (no grating) from the same bar are also shown for comparison (dashed curve).

was narrower than for any earlier antimonide mid-IR laser pumped far above threshold, apart from external cavity devices.<sup>4</sup> Fig. 2 illustrates PCDFB and Fabry-Perot spectra at several temperatures, where the Fabry-Perot linewidths range from 43 nm full width at half maximum (FWHM) at 180 K to 69 nm at 240 K, and the linewidths of α-DFB lasers fabricated from the same wafer<sup>2</sup> have similar values. At T = 180 K, where the gain spectrum of the active region comes into resonance with the grating, the PCDFB emission collapses to a single line (FWHM = 10 nm centered at 4.59 μm). At higher temperatures, the emission switches to a second line at λ = 4.70 μm (FWHM = 7 nm at 240 K). The lines exhibit a rather slow temperature variation in contrast with the α-DFB emission, which follows the temperature shift of the gain spectrum.

By combining the measured far-field profiles with TDFT-simulated near-field characteristics,<sup>1,3</sup> and taking the beam to be diffraction limited along the fast axis, we derive etendues as a function of stripe width W and plot them in Fig. 3 for α-DFB and PCDFB lasers from the same material. While both structures display diffraction-limited emission for W = 50 μm, the PCDFB etendue is lower by a factor of 5 at W = 200 μm.



**CTuE3 Fig. 3.** Etendue (in units of the diffraction limit: DL = λ/π) as a function of Gaussian stripe width for PCDFB (solid points) and α-DFB (open points) lasers fabricated from the same wafer. Operating temperatures were 180 K for the PCDFB and 160 K for the α-DFB, with both devices pumped at ten times their respective thresholds.

Although the PCDFB efficiency was roughly a factor of 2 lower than the α-DFB value, the relative brightness was still over a factor of 2 higher.

Further simulations indicate that optimized first-order PCDFB structures should display single-mode emission as well as an improved beam quality. Since the relevant figure of merit scales as the product of the threshold gain and the linewidth enhancement factor (LEF), mid-IR devices with intersubband-based quantum cascade (QCL) active regions will be especially attractive, since their LEFs are quite small. Detailed TDFT simulations project single-mode operation, and etendues no larger than twice the diffraction limit, for optimized coupling coefficients and QCL stripes as wide as 1 mm.

**References**

1. I. Vurgaftman, W.W. Bewley, R.E. Bartolo, C.L. Felix, M.J. Jurkovic, J.R. Meyer, M.J. Yang, H. Lee, and R.U. Martinelli, "Far-Field Characteristics of Mid-IR Angled-Grating Distributed-Feedback Lasers", *J. Appl. Phys.* **88**, 6997 (2000).
2. W.W. Bewley, I. Vurgaftman, R.E. Bartolo, C.L. Felix, M.J. Jurkovic, J.R. Meyer, H. Lee, R.U. Martinelli, G.W. Turner, and M.J. Manfra, "Limitations to Beam Quality of Mid-Infrared Angled-Grating Distributed-Feedback Lasers", *IEEE J. Selected Top. Quantum Electron.* **7**, 96 (2001).
3. I. Vurgaftman and J.R. Meyer, "Photonic-Crystal Distributed-Feedback Lasers", *Appl. Phys. Lett.* **78**, 1475 (2001).
4. H.Q. Le, G.W. Turner, J.R. Ochoa, M.J. Manfra, C.C. Cook, and Y.-H. Zhang, "Broad wavelength tunability of grating-coupled external cavity midinfrared semiconductor lasers", *Appl. Phys. Lett.* **69**, 2804 (1996).

**CTuE4 8:45 am**

**Measurements of α-factor in 2–2.5 μm Type-I In(Al)GaAsSb/GaSb Broadened Waveguide Lasers**

L. Shterengas, A. Gourevich, G. Belenky, State University of New York at Stony Brook, Stony Brook, NY 11794 USA, garik@ece.sunysb.edu

J.G. Kim, R. Martinelli, Sarnoff Corporation, 201 Washington Rd., Princeton, NJ 08543 USA

Mid-infrared laser applications require either coherent sources with narrow linewidths or low divergence output beams. The parameter defining both minimum spectral linewidth and beam quality is the α-factor, also called the linewidth enhancement factor or antiguiding parameter. α-factor is the ratio of the derivatives with respect to the carrier concentration of the real and imaginary parts of the media complex dielectric function. In terms of measurable quantities, it is proportional to the ratio of changes in the refractive index and modal gain with injection current.

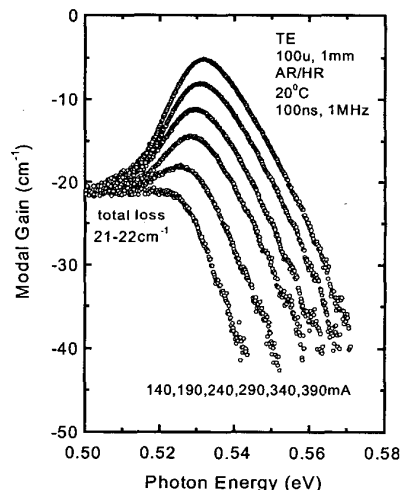
We have measured the current dependences of the α-factor spectrum of type-I 2–2.5 μm<sup>1</sup> In(Al)GaAsSb/GaSb diode lasers operating in the continuous-wave regime at room temperature. GaSb-based structures contained two compressively strained InGaAsSb QWs in active region. To keep the QW material composition out of the miscibility gap<sup>2</sup> the QW compressive strain was higher for 2.5 μm lasers than for the 2 μm de-

vices. To minimize the optical loss, the broadened waveguide laser design was used. Wafers were processed into broad stripe (100 μm) lasers, the facets were coated (0.03/0.95), and the devices were mounted p-side down on Cu heatsinks.

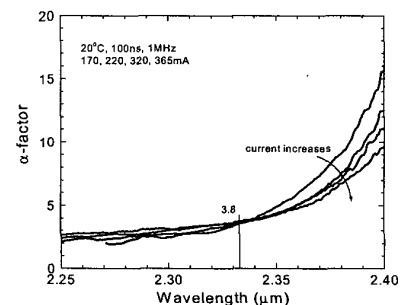
Spectra of the α-factor were obtained from the current dependence of the amplified spontaneous emission (ASE) measured from the laser front facet. A spatial filtering technique<sup>3</sup> was used to filter out ASE of the on-axis mode of 100 μm stripe width multimode lasers. Pulsed measurements were used to minimize effect of Joule heating on laser characteristics. Figure 1 shows the current dependence of the modal gain spectra of a 2.3 μm GaSb-based laser at 20°C.

The differential gain values were calculated from data presented in Fig. 1. The corresponding differential index was found through measurements of the relative shift of the Fabry-Perot modes with injection-current variations. Effect of the Joule heating was controlled by measuring the rate of the laser line shift after the threshold. Figure 2 shows the α-factor spectrum measured at different currents.

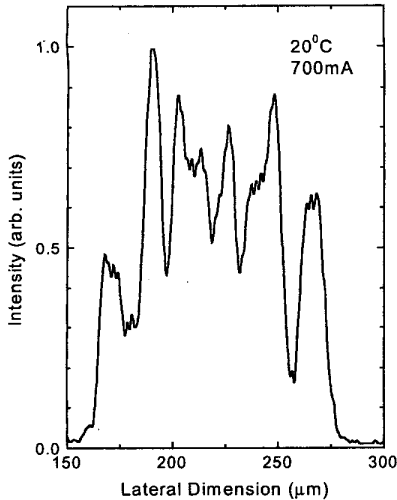
The value of the linewidth enhancement factor increases with wavelength due to differential gain decrease. The long-wavelength part of the



**CTuE4 Fig. 1.** Current dependence of the modal gain spectrum of a 2.3 μm GaSb-based laser at room temperature.



**CTuE4 Fig. 2.** Current dependence of the α-factor spectrum of 2.3 μm GaSb-based lasers at room temperature.



**CTuE4** Fig. 3. Lateral near-field emission pattern for a 2.3  $\mu\text{m}$  GaSb-based laser operating at a current  $I = 1.7I_{\text{th}}$ .

gain spectrum is related to transitions between states distant from quasi-Fermi levels and, consequently, is characterized by a lower value of the differential gain. Current increase leads to lower values of  $\alpha$  in long-wavelength part of the spectrum (Fig. 2), suggesting a faster saturation with current of the differential index compared with the differential gain. Several effects, for instance, conduction band nonparabolicity, can explain the differential index saturation.

An independent test for the value of the linewidth enhancement factor or antiguiding parameter was performed based on near-field pattern measurements. Total loss and  $\alpha$ -factor determine the laser average filament spacing  $W_F, W_F \sim (\alpha\text{-factor} \cdot \text{loss})^{-1/2}$ .<sup>4</sup> Optical losses determined from longwavelength part of the modal gain spectrum (Fig. 1) are 21–22  $\text{cm}^{-1}$  and  $\alpha$  is about 3.8 (Fig. 2). The estimated filament spacing is about 15–16  $\mu\text{m}$ . This is in agreement with the number of filaments seen in the near-field pattern of a 2.3- $\mu\text{m}$  laser operated at 1.7 times threshold (Fig. 3). 7–8 filaments are observed in the near field pattern of the device with 100- $\mu\text{m}$  stripe.

In conclusion, the values of the  $\alpha$ -factor for 2–2.5  $\mu\text{m}$  InGa(Al)AsSb QW lasers at threshold were in the range 3–4 and are in agreement with values obtained from above-threshold near-field measurements.

This work was supported by AFOSR, grant F496200110108.

## References

- D.Z. Garbuzov, H. Lee, V. Khalfin, R. Martinelli, J.C. Connolly, G.L. Belenky "2.3–2.7 mm room temperature CW operation of InGaAsSb/AlGaAsSb broad waveguide SCH-QW diode lasers" *IEEE Photon. Tech. Lett.* 11 (1999), p. 794.
- K. Shim, H. Rabitz, P. Dutta, "Band gap and lattice constant of  $\text{Ga}_x\text{In}_{1-x}\text{As}_y\text{Sb}_{1-y}$ ", *J. Appl. Phys.* 88 (2000), p. 7157.
- D.V. Donetsky, G.L. Belenky, D.Z. Garbuzov, H. Lee, R.U. Martinelli, G. Taylor, S. Luryi, J.C. Connolly "Direct measurements of heterobarrier leakage current and modal gain in

2.3  $\mu\text{m}$  double QW p-substrate InGaAsSb/AlGaAsSb broad area lasers" *IEEE Electron. Lett.* 35 (1999), p. 298.

- D. Mehuys, R.J. Lang, M. Mittelstein, J. Salzman, A. Yariv, "Self-stabilized nonlinear lateral modes of broad area lasers", *IEEE J. Quantum. Electron.* 23 (1987), p. 1909.

**CTuE5**

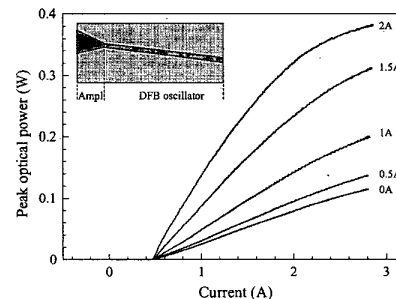
9:00 am

## Quantum Cascade Semiconductor Amplifiers for High Power Single Mode Emission at $\lambda \approx 7.5 \mu\text{m}$

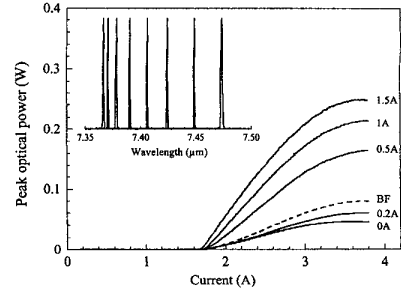
Mariano Troccoli, Federico Capasso, Claire Gmachl, Axel Straub, Deborah L. Sivco, and Alfred Y. Cho, Bell Laboratories, Lucent Technologies, 600 Mountain Ave. Murray Hill NJ 07928, Email: troccoli@lucent.com

We present a mid-IR semiconductor optical amplifier based on a quantum cascade (QC) active region, which has been used to attain high output powers from distributed-feedback (DFB) QC lasers without affecting their single mode behavior. The QC layer structure is the same as outlined in ref [1]. The device was realized as schematically shown in the inset of Fig. 1, i.e. in a master oscillator—power amplifier (MOPA) configuration. The oscillator is a 16  $\mu\text{m}$  wide, 2 mm long ridge waveguide where the single mode laser action is achieved by wet-etching a first-order Bragg grating in the topmost layer of the waveguide.<sup>2</sup> The power amplifier is a linearly tapered structure with no grating on top, 0.5 mm long and with a final width of 100  $\mu\text{m}$ . Selective current injection in the different sections is achieved by separate contact areas. In order to keep a high (>30 dB) side mode suppression ratio and to avoid the use of low-reflectivity ( $R < 0.1\%$ ) coatings on the amplifier facet, the MOPA structure is tilted at a 7° angle to the crystal lattice, so that the light reflected by the cleaved facets does not couple back into the waveguide.<sup>3</sup>

Figure 1 shows the optical power-current characteristics of sample D2744. The maximum peak power emitted from the front facet is 0.39 W. The curves were corrected for current leakage by measuring the resulting voltage on the laser section when current flows into the amplifier. From the knowledge of the current-voltage characteristics of the laser it was possible to estimate the amount of current that leaks from the amplifier



**CTuE5** Fig. 1. Light-current characteristics of sample D2744 at  $T = 80 \text{ K}$ . Duty cycle is 0.05%. Different values of the amplifier current ( $I_a$ ) are shown. Inset: schematics of the MOPA device.



**CTuE5** Fig. 2. Light-current characteristics of D2743 at 300 K for different values of  $I_a$ . Dashed line: back facet emission at  $I_a = 0$ . Inset: Emission spectra measured at (from left to right): 10, 50, 80, 120, 160, 200, 250, and 300 K.

to the laser during the light-current characterization.

Figure 2 shows the light-current characteristics obtained from sample D2743 at  $T = 300 \text{ K}$ . The amplifier section in this case is smaller, to avoid overheating of the device at high currents. Its length is 0.28 mm and the maximum width is 52  $\mu\text{m}$ . The measurement of the back facet emission in this case allowed us to estimate the maximum amplification and the waveguide losses which turned out to be 4.9 dB and 22.1  $\text{cm}^{-1}$ , respectively. In the inset of Fig. 2 are plotted the spectra measured from sample D2744 at temperatures varying from 10 to 300 K at currents corresponding to the peak optical power. The attainment of single mode operation in a large temperature range, facilitated by the tilted design, yields a wide tunability of the emission. Far-field measurements performed on D2743 showed that 90% of the optical power is concentrated within an angle of 20°, in the plane of the epitaxial layers. This value is significantly lower than the beam divergence ( $\sim 60^\circ$ ) measured with smaller ridges<sup>4</sup> owing to the weaker diffraction from the wider amplifier facet. Moreover, the transverse beam shape is not affected by the width of the cavity, as it happens in other high-power single-mode devices.<sup>5</sup>

- C. Gmachl, A. Tredicucci, F. Capasso, A.L. Hutchinson, D.L. Sivco, J.N. Baillargeon, and A.Y. Cho, "High power  $\lambda \approx 8 \mu\text{m}$  quantum cascade lasers with near optimum performance", *Appl. Phys. Lett.* 72, 3130–3132 (1998).
- C. Gmachl, F. Capasso, J. Faist, A.L. Hutchinson, A. Tredicucci, D.L. Sivco, J.N. Baillargeon, S.N.G. Chu, and A.Y. Cho, "Continuous-wave and high-power pulsed operation of index-coupled distributed feedback quantum cascade laser at  $\lambda \approx 8.5 \mu\text{m}$ ", *Appl. Phys. Lett.* 72, 1430–1432 (1998).
- C.E. Zah, J.S. Oshinski, C. Caneau, S.G. Menocal, L.A. Reith, J. Zalsman, F.K. Shokoohi, and T.P. Lee, "Fabrication and performance of 1.5  $\mu\text{m}$  GaInAsP travelling-wave laser amplifier with angled facets", *Electron. Lett.* 23, 990–991 (1987).
- C. Gmachl, F. Capasso, A. Tredicucci, D.L. Sivco, R. Kohler, A.L. Hutchinson, and A.Y. Cho, "Dependence of the device performance on the number of stages in quantum-cascade lasers", *IEEE J. Sel. Topics Quantum Electron.* 5, 808–816 (1999).